Conference Paper, Published Version

Iimura, Kotaro; Shibayama, Tomoya; Takabatake, Tomoyuki; Esteban, Miguel; Ishii, Hidenori; Hamano, Go

Laboratory Study of Tsunami Behavior around Two Upright Sea Dikes with Different Heights

Coastal Structures 2019 - Nils Goseberg, Torsten Schlurmann (eds) - © 2019 Bundesanstalt für Wasserbau
ISBN 978-3-939230-64-9 (Online) - DOI: 10.18451/978-3-939230-64-9_048

Laboratory Study of Tsunami Behavior around Two Upright Sea Dikes with Different Heights

K. Iimura, T. Shibayama, T. Takabatake, M. Esteban, H. Ishii, & G. Hamano
Department of Civil and Environmental Engineering, Waseda University, Tokyo, Japan

Abstract: The *2011 Tohoku Tsunami* caused severe damage to areas where two adjacent upright sea dikes of different heights met. The height of an upright sea dike along the Japanese coastline is generally designed based on data from past tsunami or storm surge events, so their height differs along the coastline and there are places where dikes of different heights meet. In this study, the authors aim to investigate the tsunami flow around such dikes by means of both three-dimensional hydraulic experiments and numerical simulations. The laboratory experiments were conducted in the tsunami wave basin of Waseda University, where twelve experimental cases were tested by changing the heights of each side of the dike model and the waveforms. The results show that the difference in height between two adjacent sections of a dike influences the volume of overtopping, and especially, the extent of the inundation. Many cross-section changing dikes exist along the coastlines of Japan, and it might be necessary to re-assess the effectiveness of these dikes against tsunami hazards in many parts of this country, and possibly others.

Keywords: 2011 Tohoku Tsunami, cross-section changing dikes, overtopping, inundation, hydraulic experiment, numerical simulation, Particle Image Velocimetry

1 Introduction

The *2011 Tohoku Earthquake and Tsunami* devastated the Tohoku region in northern Japan, destroying coastal defenses and flooding the extensive area behind the dikes that protected the coastline. The design height of a sea dike prior to this event was generally established based on the highest waves that affected an area, which were recorded during past tsunami or storm surge events (in the Tohoku region, generally past tsunami events such as the *1896 Sanriku Earthquake*, *1933 Sanriku Earthquake*, and *1960 Valdivia Earthquake* were used). As the design height was determined in each administrative district, they differ along the coastline (especially at the administrative boundary), creating places where dikes of different heights (and shapes) meet. Also, the design codes that were used varied according to the government office that manages each section of the coast.

According to the damage report of the *2011 Tohoku Earthquake and Tsunami* by the National Institute for Land and Infrastructure Management (NILIM) (2011) of Japan and Sato et al. (2011), severe damage was observed at places where two sea dikes of different cross-section met (herewith referred to as cross-section changing dikes). There are a number of patterns of cross-section changing dikes, and for example sometimes two adjacent upright dikes of different heights meet, whereas in others two adjacent trapezoid dikes of different heights join, or an upright dike is located adjacent to a water gate. In such cases, typically the dike with the smaller cross-section is destroyed around the point where the cross-section changes.

In this sense, Tajima et al. (2013) conducted numerical simulations of inundation behind cross-section changing dikes in order to evaluate their effectiveness against overtopping tsunamis. The result of the water level and velocity vector analysis showed that the overtopping flow accumulated at the point where the cross-section changes. As a result, the volume of overtopping increases over the

lower part of the dike, and correspondingly decreases over the higher dike. However, these authors did not carry out any laboratory tests, and to date little work has been done on this particular issue. Esteban et al. (2009, 2015) conducted laboratory experiments on the changing patterns of tsunami attack on breakwaters of different cross-sections, showing how damage patterns could indeed increase for transition sections where a caisson breakwater is protected by tetrapod armour and others where no tetrapods are present. However, such work only considered breakwaters, and did not attempt to establish the inundation patterns behind the dikes. Other work such as that of Esteban et al. (2017) looked at tsunami overtopping of structures in the laboratory, but only considered two dimensional problems.

Nevertheless, to date the tsunami flow around cross-section changing dikes has not received enough attention in the literature and, to the authors' best knowledge, no three-dimensional hydraulic experiments have been conducted on such flows. Therefore, in this study, the authors aim to investigate the tsunami flow around cross-section changing dikes through the use of hydraulic experiments. Specifically, the objectives of this study are:

- Examining different patterns of flows that overtop cross-section changing dikes.
- Studying the influences of the difference in height between two adjacent dikes on the volume of overtopping and the extent of inundation.

Thus, in the present study the authors focused on two adjacent upright dikes of different heights, looking at a case study location situated in the coastlines of Nakoso District in Fukushima prefecture, where the dike height changed from 4.20 m to 6.00 m (Fig. 1). Here, the report of NILIM (2011) indicated that the 2011 tsunami destroyed the sea dike with the lower height and increased flood damage to the area behind it.

Fig. 1. Photograph of the cross-section changing dike in Nakoso District in Fukushima prefecture, Japan: (a) seaside view (b) landside view (NILIM (2011)).

2 Methodology

2.1 Experimental Setup

2.1.1 Tsunami Wave Basin Description

Laboratory experiments were conducted in the tsunami wave basin (TWB) of Waseda University in Tokyo, Japan (dimensions 4.00 m × 9.00 m × 0.50 m, as shown in Fig. 2). A vertical reservoir is attached to one end of TWB, controlled by a vacuum pump and air valves that can create suction type dam-break waves. A bed topography consisting of a 1:10 slope and a flatbed (with a constant height of 0.20 m from the bottom of the TWB) behind the slope was used for the experiments, representing a typical shoreline in Japan. The bed was made of stainless steel and the tip of the slope was located 4 m from the reservoir. The still water level was kept at 0.17 m for all experimental conditions.

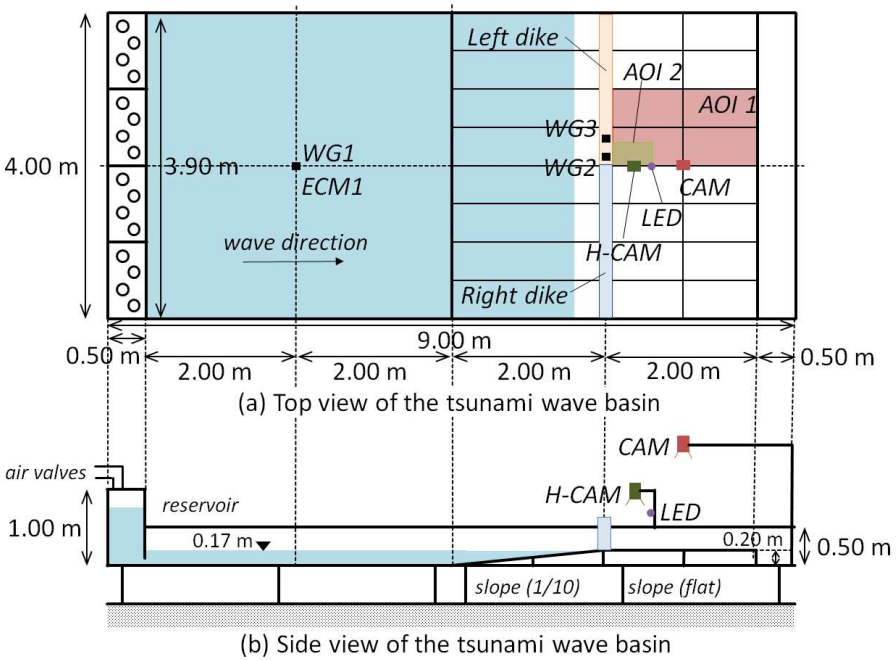

Fig. 2. Apparatus and layout of the laboratory experiments: (a) top view; (b) side view.

2.1.2 Dike Models

The dike models were made of lauan plywood (coated in urethane, in order to make it waterproof), glued onto the wave basin by silicone sealant. The dike models were placed 6.00 m away from the reservoir, where the bed topography changes from the 1:10 slope to the flat bed (Fig. 2). The dike models represented the typical upright dikes that are ubiquitous along Japanese coastlines, using a 1:50 scale. The dike height combinations used were 0.08 m – 0.08 m (dike model A, no height difference), 0.08 m – 0.12 m (dike model B), and 0.08 m – 0.40 m (dike model C) (Fig. 3). Essentially, looking from the reservoir towards the "land side of the basin", the height of the left side of the dike was kept at a height of 0.08 m for all experimental conditions (orange shaded dike in Figs. 2 and 3), while the right part varied between 0.08 m and 0.40 m (blue shaded dike).

The two adjacent dikes were connected to each other at the middle point of the TWB (i.e. at 1.95 m from each side wall). This connecting point will be referred to as the cross-section changing point hereafter. The 0.08 m – 0.08 m dike model was used as a reference and was compared to the results of the other two models. The cross-section changing dike of Nakoso District in Fukushima prefecture, Japan (Fig. 1, height change of 4.20 m to 6.00 m) was used as a reference for the 0.08 m – 0.12 m dike model. In the case of the 0.08 m – 0.40 m model, the 0.40 m dike was high enough to prevent any overtopping, so that the flow only overtops the low 0.08 m section of the dike.

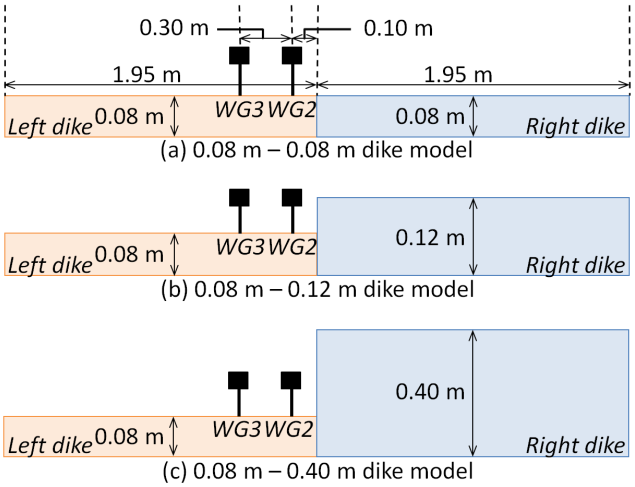

Fig. 3. Model layout and measurement apparatus in each type of dike model: (a) 0.08 m – 0.08 m dike model A; (b) 0.08 m – 0.12 m dike model B; (c) 0.08 m – 0.40 m dike model C.

2.1.3 *Instrumentation and measuring apparatus*

A summary of the instruments used in the experiments is shown in Tab. 1. The water level above the low 0.08 m dike was recorded using two wave gauges (WGs), as shown in Figs. 2 and 3. One was set 0.10 m from the cross-section changing point (WG2) and the other 0.30 m to the side of it (WG3). WG1 was placed in front of the dikes, to measure the wave profile as it propagated towards them. The velocity at the point of WG1 was recorded using an electromagnetic current meter (ECM1). ECM1 was submerged in water (it was set 0.10 m from the bottom of the TWB to avoid contact with air during the propagation of the wave, as these types of instruments appear not to produce good results when situated outside of water, see Esteban et al. (2017)). The sampling frequency of the WGs and ECM1 was 100 Hz, and were all connected to a data acquisition system (DAS).

A plan view of the leading edge of the inundation was recorded using a high-resolution video camera (CAM, 1920 px × 1080 px resolution). The area of interest (AOI 1) for the CAM recordings is shown as the red shaded area in Fig. 2. This study focuses on the inundation behind the orange shaded lower section of the dike. From the recordings, the area of inundation was calculated for each time step using the open source image processing software ImageJ (version 1.51, a public domain Java-based image processing program developed by Wayne Rasband (National Institute of Health)).

The flow behind the cross-section changing point and the landward area behind the low section of the dike were recorded using a high-speed camera (H-CAM, 1024 px × 1024 px resolution). The area of interest (AOI 2) for the H-CAM recordings is shown as the green shaded area in Fig. 2. The flow velocity field was analyzed using Particle Image Velocimetry system (PIV) developed by KATOKOKEN Co. Ltd. According to Goseberg and Schlurmann (2014), the usage of PIV is effective for analyzing the velocity fields of the water surface in the near-field of a structure.

The CAM and H-CAM recordings were synchronized with the hydrodynamic data of WGs and ECM1 using an LED light, in a similar way to what is described by Stolle et al. (2019). The LED light was also connected to the DAS, and the light bulb was placed so that it can be observed in each video recordings. The timing of the moment when the light bulb was lit in the video recording and the timing when the DAS marked the voltage signal of the LED light is the same, allowing for the data to be synchronized.

Table 1. Summary of measuring apparatus and instrumentation.

Instrument	Manufacturer	Product	Sampling Rate	Accuracy/ Resolution
Wave gauge (WG)	KENEK Co. Ltd.	CHT6-30,40	100 Hz	Maximum error: 6.0 %
Electromagnetic current meters (ECM)	KENEK Co. Ltd.	VMT2-200-04P,04PL	100 Hz	Maximum error: 14.6 %
Data acquisition system (DAS)	KENEK Co. Ltd.	ADS2116		
Video camera (CAM)	Sony Co.	HDR-CX680	60 fps	1920 px × 1080 px
High-speed camera (H-CAM)	KATOKOKEN Co. Ltd.	High Speed Camera K4	200 fps	1024 px × 1024 px
Particle Image Velocimetry system (PIV)	KATOKOKEN Co. Ltd.	Flow Expert 2D2C		
Image processing program	Wayne Rasband (NIH)	ImageJ		

2.2 *Waveforms and experimental cases*

Twelve experimental cases were tested by changing the heights of each side of the dike model and the waveforms, using a 1:50 scale (Tab. 2). H_{1max} is the maximum incident wave height recorded at WG1, and V_{1max} is the maximum incident wave velocity recorded at ECM1. Four types of waveforms with different water level profiles (measured from the bottom of the TWB, Fig. 4 (a)) and velocities were used (Fig. 4 (b)). In this study, a suction type dam-break method was chosen for generating the incident waves. To change the waveforms, the initial water elevation inside the reservoir was adjusted from 0.90 m for Wave 1 to 0.60 m for Wave 4 (in intervals of 0.10 m). For the remainder of this paper, time t = 0.0 s refers to the moment when the wavefront of each waveform reached WG1.

The generated waveforms represent bore-like waves. Fig. 4 (c) shows the wave profiles recorded at WG2 without the dike models, in order to evaluate the hydrodynamic conditions. It should be noted that the lowest values of water level in Fig. 4 (c) starts at 0.012 m, as will be explained later in section 3.1. Tab. 3 shows the wave half period ($T_h/2$), the maximum wave height (H_{hmax}), and the wavefront velocity (V_h) for the hydrodynamic wave profiles, along with the corresponding prototype scaled values (using Froude scaling): wave half period ($T_p/2$), the maximum wave height (H_{pmax}), and the wavefront velocity (V_p). $T_h/2$ was calculated from the time when the water level exceeded 0.01 m until the moment it dropped again to 0.01 m. V_h was obtained by using the difference in the arrival times between WG2 and another WG placed 0.5 m to the landward side from WG2, following Esteban et al. (2017) and Stolle et al. (2018). This is due to the difficulties of the usage of ECM in the landside, as the wavefronts contain air bubbles and cavitation occurs around the sensor. In prototype scaling, $T_p/2$ ranged between 37.83 s and 43.49 s, H_{pmax} between 2.25 m and 3.73 m, and V_p between 9.30 m/s and 12.63 m/s. Since the wave period of *2011 Tohoku Tsunami* tended to be longer than 10 min, $T_p/2$ appears to be short. However, as this study focuses on the overtopping flow over sea dikes and the leading edge of the inundation over land, only the front part of a tsunami wave was considered. The video analyzation by Sanuki et al. (2013) estimated the wavefront velocity of *2011 Tohoku Tsunami* to be around 12 m/s to 14 m/s near the coastline. Takabatake et al. (2019) also showed that the maximum velocities of tsunami simulated near the coastline (in this case, Vancouver Island, Canada) are more than 8 m/s. Hence, the waves used in the present study appear to model reasonably well wavefront of bore-like tsunamis.

Table 2. Summary of experimental cases when the dike models were present.

Case name	Dike height combination	Type of waveform	H_{1max} (m) (WG1)	V_{1max} (m/s) (ECM1)
A-1	0.08 m − 0.08 m (A)	1	0.083	0.53
A-2	0.08 m − 0.08 m (A)	2	0.075	0.48
A-3	0.08 m − 0.08 m (A)	3	0.062	0.43
A-4	0.08 m − 0.08 m (A)	4	0.055	0.38
B-1	0.08 m − 0.12 m (B)	1	0.083	0.53
B-2	0.08 m − 0.12 m (B)	2	0.075	0.48
B-3	0.08 m − 0.12 m (B)	3	0.062	0.43
B-4	0.08 m − 0.12 m (B)	4	0.055	0.38
C-1	0.08 m − 0.40 m (C)	1	0.083	0.53
C-2	0.08 m − 0.40 m (C)	2	0.075	0.48
C-3	0.08 m − 0.40 m (C)	3	0.062	0.43
C-4	0.08 m − 0.40 m (C)	4	0.055	0.38

Table 3. Summary of experimental cases without dike models.

Type of waveform	Experimental Values			Prototype Scaled Values		
	$T_h/2$ (s)	H_{hmax} (m)	V_h (m/s)	$T_p/2$ (s)	H_{pmax} (m)	V_p (m/s)
1	6.15	0.087	1.79	43.49	4.33	12.63
2	5.90	0.076	1.56	41.72	3.80	11.03
3	5.45	0.067	1.47	38.54	3.33	10.40
4	5.35	0.057	1.32	37.83	2.85	9.30

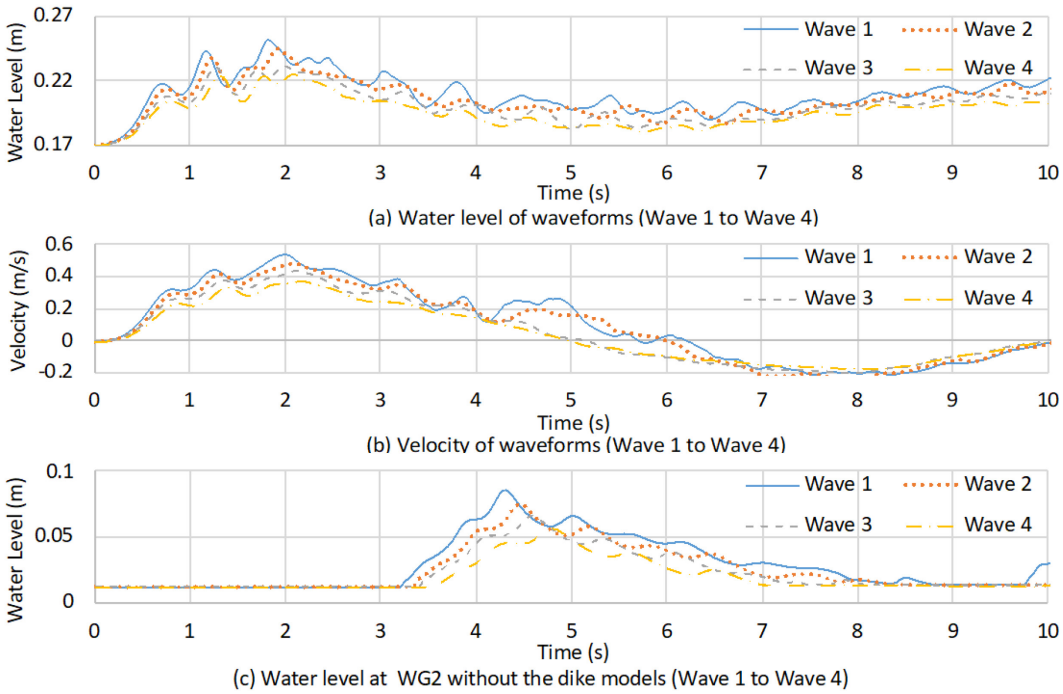

Fig. 4. (a) Water level recorded at WG1, (b) velocity recorded at ECM1, (c) the water level recorded at WG2 without the dike models for each types of waveforms: Wave 1, Wave 2, Wave 3, and Wave 4.

3 Results

3.1 Water level above the low 0.08 m dike

The water level above the low 0.08 m dike for all 12 experimental cases at WG2 and WG3 is shown in Fig. 6. The maximum water level above the low 0.08 m dike (H_{2max} for WG2 and H_{3max} for WG3) is shown in Fig. 5. It should be noted that each WG has a wire stopper at the bottom and that the wire section starts 0.012 m above it, and thus they cannot record water level lower than 0.012 m. Therefore, the lowest values in Fig. 6 starts at 0.012 m. Camera recordings and visual observations indicate that the water level recordings between t = 4.5 s and t = 5.0 s in Fig. 6 are caused by vertical splash, a phenomenon which is outside of the scope of this study. Therefore, the maximum water level in Fig. 5 considers only values that took place between t = 5.0 s and t = 6.5 s.

The results of Figs. 5 and 6 indicate that the change in cross-section has an influence on the water level over the low 0.08 m section of the dike. Among the three dike model combinations, the 0.08 m – 0.40 m dike model (combination C) resulted in a higher water level at WG2 compared to the other two combinations. On the other hand, no clear difference was observed at WG3. Thus, the recordings at WG2 and WG3 indicate that the flow accumulated at the point where the dikes changed section.

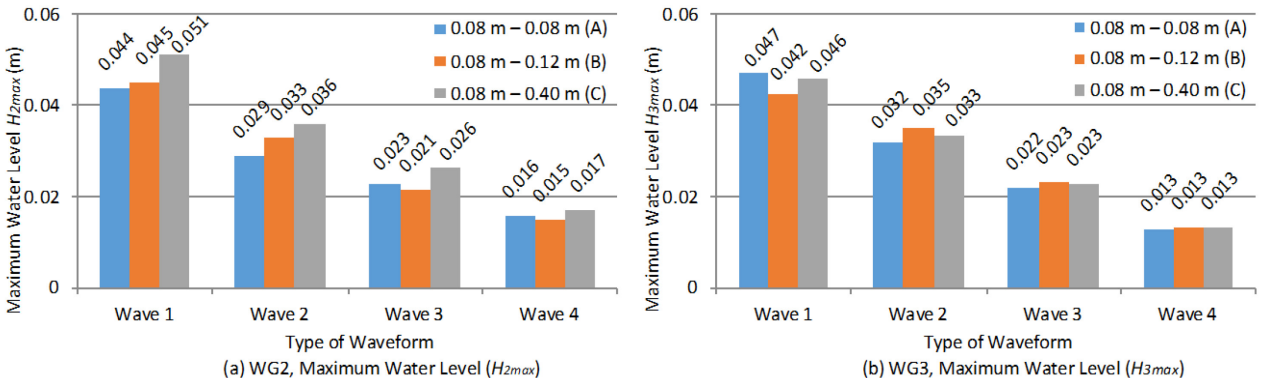

Fig. 5. a) Maximum water level recorded at WG2 (H_{2max}) and b) WG3 (H_{3max}) .

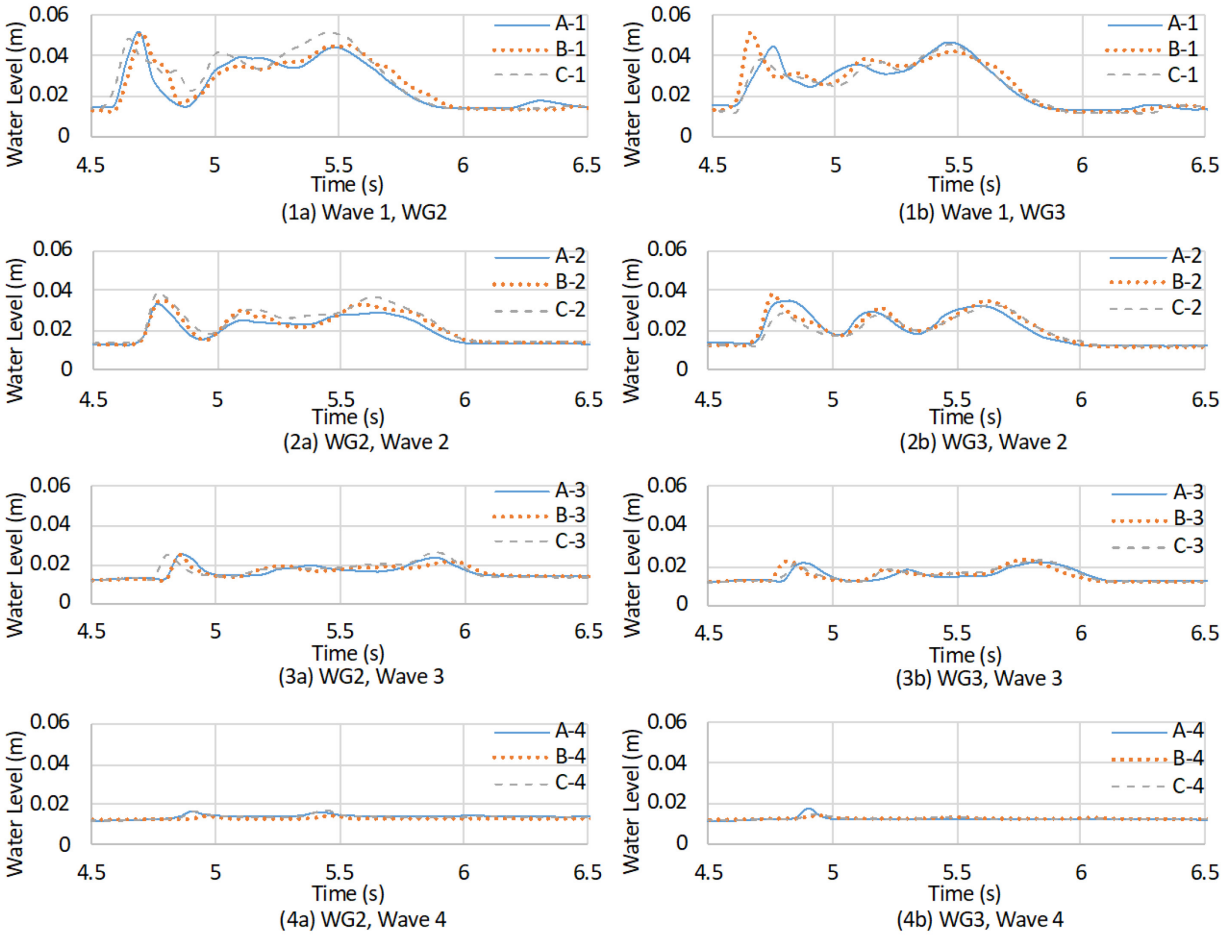

Fig. 6. Water level over the low 0.08 m for Wave 1: (1a) WG2; (1b) WG3, for Wave 2: (2a) WG2; (2b) WG3, for Wave 3: (3a) WG2; (3b) WG3, and for Wave 4: (4a) WG2, (4b) WG3.

3.2 Plan view of the leading edge of inundation

The CAM recordings showed that the inundation over the 0.08 m – 0.12 m dike configuration (combination B) advanced quicker than in the other two model setups. Fig. 7 shows the inundation of representative cases (A-4, B-4, and C-4), along with the area recorded within AOI 1 (delimitated by a red rectangle in Figs. 2 and 7). The inundation area behind the lower 0.08 m section of the dike was calculated using ImageJ, and is shown as the yellow shaded area. The extent of the inundation inside AOI 1 for each time step in the CAM recordings was delimitated by manually placing numerous dots around it, before processing the image. Although the area of inundation was larger at t = 5.0 s for case C-4 compared to the other two, it became smaller after t = 6.0 s. This is due to the existence of 0.40 m dike that prevented any overtopping and allowed the flow to only overtop the lower 0.08 m dike. Essentially, in this case the accumulated flow piled up and increased the inundation speed inside AOI 1, especially in areas right behind the lower section of the dike.

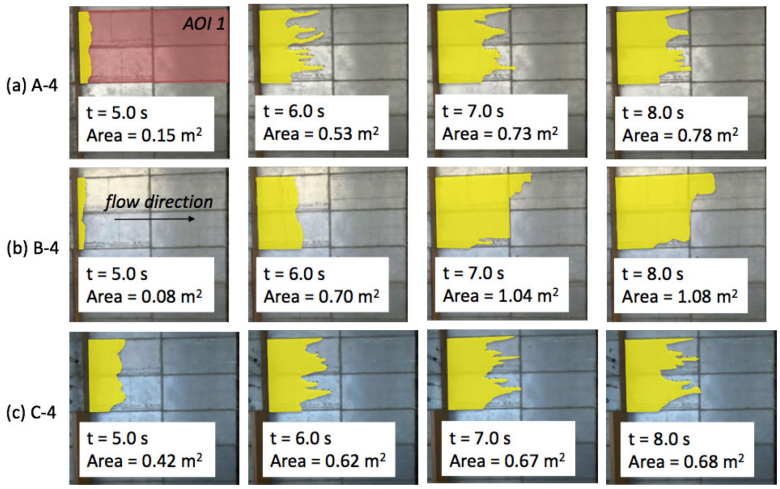

Fig. 7. The change in inundation area from t = 5.0 s to t = 8.0 s for Wave 4: (a) A-4; (b) B-4; (c) C-4.

3.3 Flow velocity field

The flow velocity field behind the cross-section changing dikes was analyzed using a PIV software, FlowExpert 2D2C (KATOKOKEN Co. Ltd.). In this study, the time interval of H-CAM recordings was 0.005 s, and no tracer particles were used since there were enough air bubbles in the flow to trace to the water movement and calculate the velocity field. Similarly to the CAM recordings, the results of the PIV analysis also show that the velocity field behind the low section of the dike is highly influenced by the change in cross-section and the type of waveform. Fig. 9 shows the time history of the average velocity behind the low 0.08 m dike (AOI 2) for each type of waveforms. In order to evaluate the intensity of the integrated velocity field throughout AOI 2, the average velocity inside the whole area was calculated. Fig. 8 shows the maximum velocity (V_{Pmax}) recorded for each experimental case.

Figs. 8 and 9 indicated how the difference in height greatly influences the flow velocity over a wide area, along with the maximum velocity inside AOI 2. Also, the results of Figs. 8 and 9 show that the flow velocity decreased as the wave height decreased for the 0.08 m – 0.08 m dike configuration (combination A). On the other hand, the flow velocity behind the low side of dike did not reduce proportionally with decreases in the incident wave heights for the 0.08 m – 0.12 m dike (B) and the 0.08 m – 0.40 m dike (C). In cases B-1, B-2, and B-3, almost no reduction in the flow velocity was observed. In cases C-1, C-2, and C-3, the flow velocity increased gradually from 0.42 m/s to 0.66 m/s, in spite of the decrease in incident wave heights, perhaps due to the existence of the 0.40 m dike that did not allow any overtopping and increased the accumulation of the flow into the low 0.08 m section of the dike. This result agrees with the result of CAM recordings in Fig. 7, where a rapid inundation was observed in areas right behind the lower section of the dike for case C-4. The sudden decrease in velocity for Wave 4 is due to the small amount of overtopping, compared to the other three incident waves (Fig. 6). Thus, the PIV results indicate that the difference in height between each side of the dike clearly affects the flow velocity field behind the lower dike.

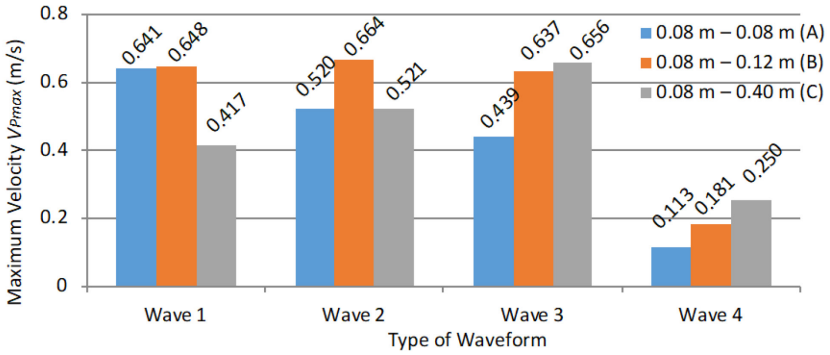

Fig. 8. Maximum velocity recorded through the PIV analysis (V_{Pmax}) at AOI 2 for each type of waveforms.

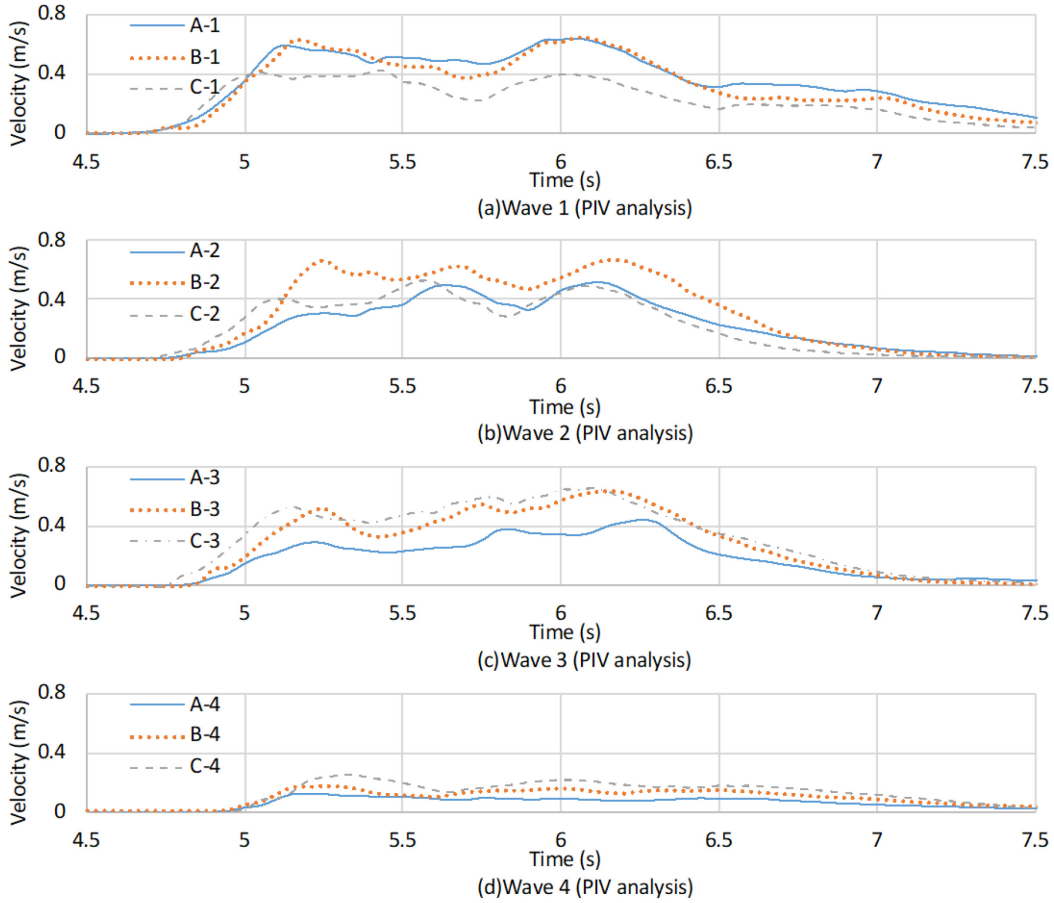

Fig. 9. Average velocity within the velocity field behind the low 0.08 m dike (AOI 2) for each type of waveform: (a) Wave 1, (b) Wave 2, (c) Wave 3, and (d) Wave 4 (according to PIV analysis).

4 Discussion

The study examined the effect of cross-section changing dikes on tsunami overtopping. The experimental results at WG2 indicate that the difference in height between the two dikes increases the volume of overtopping over the lower part of the dike, which agrees with Tajima et al. (2013). Furthermore, the overtopping flow seems to accumulate specifically at the cross-section changing point, since no clear difference was observed at WG3 (which is located farther away from the cross-section changing point than WG2). For the dike configuration with a height difference (combination B and C), the leading edge of inundation advanced quicker, and the flow velocity behind the low side of dike did not reduce proportionally with decreases in the incident wave heights. These results suggest that cross-section changing dikes could result in increased inundation damage behind them, as highlighted by the actual recorded damage around the cross-section changing dike in Nakoso district during the 2011 event (NILIM (2011)) (Fig. 1).

The *2011 Tohoku Earthquake and Tsunami* is considered to be a level 2 tsunami, which takes place infrequently (with return periods of over 1,000 years), but can cause high inundation heights (typically over 10 m) that devastate coastal areas (Shibayama et al. (2013)). The experimental results of the leading edge of the inundation in AOI 1 along with flow velocity field in AOI 2 (areas much closer to the dikes) in this study indicates the consequences of inundation in areas right behind the low section of cross-section changing dikes. Quicker inundation in such areas highlights the dangers of scouring and the failure of buildings and structures in the areas just behind dikes with relatively smaller cross-section. Therefore, in order to protect the settlements and facilities not just in the Tohoku region, but throughout the Japanese coastline against future level 2 tsunamis, re-assessment of such dikes is needed.

Although the actual mechanism of the collapse of cross-section changing dikes was outside of the scope in the present study, damage reports by NILIM (2011) and Sato et al (2011) highlight not only the inundation behind such dikes, but also that the lower dikes suffered damage around the cross-section changing point. Therefore, consideration of the wave-induced forces on cross-section changing coastal structures represents an important area of future research.

5 Conclusion

In conclusion, the study found that the difference in height between two adjacent dikes clearly influences the volume of overtopping and, especially, the extent of the inundation. Due to such differences in dike heights, the speed of inundation and the flow velocity do not reduce proportionally as the incident wave heights decreases.

Cross-section changing dikes exist not only along the coastlines of the Tohoku area, but also in other locations such as the Tokyo Bay. Hence, based on the results of this study it is necessary to re-assess the effectiveness of these dikes against tsunami events in many parts of Japan.

6 Acknowledgments

The present work was performed as a part of activities of Research Institute of Sustainable Future Society, Waseda Research Institute for Science and Engineering, Waseda University. Furthermore, the work is financially supported by the grant from Penta-Ocean Construction Co., Ltd (B2R500027001).

References

Esteban, M., Glasbergen, T., Takabatake, T., Hofland, B., Nishizaki, S., Nishida, Y., Stolle, J., Nistor, I., Bricker, J., Takagi, H. and Shibayama, T., 2017. Overtopping of Coastal Structures by Tsunami Waves. Geosciences, 7(4), 121.

Esteban, M., Thao, N. D., Takagi, H., Jayaratne, R., Mikami, T. and Shibayama, T., 2015. Stability of Breakwaters Against Tsunami Attack. Handbook of Coastal Disaster Mitigation for Engineers and Planners. Esteban, M., Takagi, H. and Shibayama, T. (eds.). Butterworth-Heinemann (Elsevier); Oxford, UK.

Esteban, M., Danh Thao, N., Takagi, H., Shibayama, T., 2009. Pressure exerted by a solitary wave on the rubble mound foundation of an armoured caisson breakwater, in: 19th International Offshore and Polar Engineering Conference, Osaka, Japan.

Goseberg, N., Schlurmann, T., 2014. Non-stationary flow around buildings during run-up of tsunami waves on a plain beach, in: Coastal Engineering Proceedings 34.

National Institute for Land and Infrastructure Management (NILIM), 2011. Quick Report to Damage to Infrastructures by the 2011 off the Pacific coast of Tohoku Earthquake. Technical Note of National Institute for Land and Infrastructure Management, 646, 86-241 (in Japanese).

Sanuki, H., Takemori, R., Tajima, Y., and Sato, S., 2013. Study on tsunami flooding in river based on video images and numerical simulation. Journal of Japan Society of Civil Engineers, Ser. B2 (Coastal Engineering), 69(2), I_196-I_200 (in Japanese).

Sato, S., Takewaka, S., Liu, H., Nobuoka, H., 2011. Tsunami damages of Nakoso coast due to the 2011 Tohoku Pacific Ocean Earthquake. Journal of Japan Society of Civil Engineers, Ser. B2 (Coastal Engineering), 67(2), I_1296-I_1300 (in Japanese).

Shibayama, T., Esteban, M., Nistor, I., Takage, H., Danh Thao, N., Mastumaru, R., Mikami, T., Aranguiz, R., Jayaratne, R., Ohira, K., 2013. Classification of tsunami and evacuation areas. Natural Hazards, 67, 365-386.

Stolle, J., Takabatake, T., Hamano, G., Ishii, H., Iimura, K., Shibayama, T., Nistor, I., Goseberg, N., Petriu, E., 2019. Debris transport over a sloped surface in tsunami- like flow conditions. Coastal Engineering Journal, 61(2), 241-255.

Stolle, J., Takabatake, T., Nistor, I., Mikami, T., Nishizaki, S., Hamano, G., Ishii, H., Shibayama, T., Goseberg, N., Petriu, E., 2018. Experimental investigation of debris damming loads under transient supercritical flow conditions. Coastal Engineering, 139, 16-31.

Takabatake, T., St-Germain, P., Nistor, I., Stolle, J., Shibayama, T. 2019. Numerical modelling of coastal inundation from Cascadia Subduction Zone tsunamis and implications for coastal communities on western Vancouver Island, Canada, Natural Hazards, 1-25.

Tajima, Y., Funatake, S., Sato, S., 2013. Disaster reduction function of seawalls against overflowing catastrophic tsunami. Journal of Japan Society of Civil Engineers, Ser. B2 (Coastal Engineering), 69(1), 23-33 (in Japanese).